Microfluidics

Deutsche Ausgabe: DOI: 10.1002/ange.201505294
Internationale Ausgabe: DOI: 10.1002/anie.201505294

High-Throughput, Label-Free Isolation of Cancer Stem Cells on the Basis of Cell Adhesion Capacity**

Yuanqing Zhang, Minhao Wu, Xin Han, Ping Wang, and Lidong Qin**

Abstract: *Herein we report a microfluidics method that enriches cancer stem cells (CSCs) or tumor-initiating cells on the basis of cell adhesion properties. In our on-chip enrichment system, cancer cells were driven by hydrodynamic forces to flow through microchannels coated with basement membrane extract. Highly adhesive cells were captured by the functionalized microchannels, and less adhesive cells were collected from the outlets. Two heterogeneous breast cancer cell lines (SUM-149 and SUM-159) were successfully separated into enriched subpopulations according to their adhesive capacity, and the enrichment of the cancer stem cells was confirmed by flow cytometry biomarker analysis and tumor-formation assays. Our findings show that the less adhesive phenotype is associated with a higher percentage of CSCs, higher cancer-cell motility, and higher resistance to chemotherapeutic drugs.*

Accurate isolation and better understanding of cancer stem cells (CSCs) are very important in basic and clinical cancer research.[1] They are also key factors for the development of novel therapeutic strategies.[2] Current methods for the isolation of CSCs largely rely on CSC-specific cell-surface markers or long-term culture; however, the CSC-specific cell surface markers remain unclear in many cancer types.[3] Label-free CSC enrichment methods may be able to replace biomarker-based isolation and have broad application to different cancer types. Recently, it was reported that isolated CSC populations tend to re-express all the original general markers and reverse themselves to a mixed population after days of cultivation. Cancer cells may transform phenotypes stochastically.[4] Given the challenge in both obtaining and maintaining CSCs, an efficient, rapid, and convenient CSC-enrichment method is desirable.

Several studies have revealed a relationship between adhesiveness and stemness in keratinocytes and human mammary epithelial cells.[5] Because CSCs are cancer cells that possess characteristics associated with normal stem cells, we used cell adhesiveness as a biophysical marker to make a tool for CSC isolation. Microfluidic systems provide unique opportunities to investigate the influence of physical (adhesiveness) and biological (phenotype) parameters on advanced-stage cancer.[6] By using microfabrication technology, we designed a unique cell-purification system to enrich the less adhesive subpopulation of breast-cancer and melanoma cells. The separation device, which we termed a high-throughput cell-adhesion chip (HCA-Chip; Figure 1), employs artificial microchannels in combination with hydrodynamic force and adhesive extracellular-matrix materials to separate less adhesive cells from parental cells.

Our experiments demonstrate the effectiveness of the HCA-Chip for separating the following cells into enriched subpopulations of low and high adhesive capacity: 1) eight breast-cancer cell types with distinct adhesive capacity and metastatic potential, and 2) two heterogeneous breast-cancer cell lines (SUM-149 and SUM-159). The low-adhesive phenotype was associated with a higher percentage of CSCs, higher cancer-cell motility, and increased resistance to chemotherapeutic drugs. We also used the mammosphere formation efficiency assay and flow cytometry to assess the tumorigenicity of the subpopulations of SUM-149 and SUM-159 cells. Our study provides an example of how a microfluidics-based approach can be used for CSC and cancer-metastasis research. To the best of our knowledge, it is the first time that cell adhesiveness has been used as a biophysical marker to effectively isolate cancer stem cells.

In a typical experiment, the HCA-Chip was fabricated with poly(dimethylsiloxane) (PDMS) by a photolithographic process, as described previously (see Figure S1 in the Supporting Information).[7] The HCA-Chip contained two layers: the PDMS layer and a $75 \times 50\ mm^2$ glass slide that was coated with a thin polystyrene layer (see Figure S2). This treatment increased protein adsorption onto the surface of the glass slide. The PDMS layer consisted of eight microchannels, and the depth of each microchannel can be set to any size from 25 to 60 μm (see Figure S3). The depth was controlled by changing the fabrication procedure. To mimic the cell-

[*] Y. Zhang,[+] X. Han, L. Qin
Department of Nanomedicine
Houston Methodist Research Institute
Houston, TX 77030 (USA)
E-mail: LQin@houstonmethodist.org
Y. Zhang,[+] X. Han, L. Qin
Department of Cell and Developmental Biology
Weill Medical College of Cornell University
New York, NY 10065 (USA)
M. Wu[+]
Department of Immunology, Zhongshan School of Medicine
Sun Yat-sen University
74 Zhongshan 2nd Road, Guangzhou 510080 (China)
P. Wang
Department of Pathology and Genomic Medicine
Houston Methodist Research Institute
Houston, TX 77030 (USA)
E-mail: pwang@houstonmethodist.org
[+] These authors contributed equally.

[**] This study was funded by the Cancer Prevention and Research Institute of Texas (CPRIT-R1007), the NIH-CA180083, the Emily Herman Research Fund, and the Golfers Against Cancer Foundation.

Supporting information for this article, including experimental details, is available on the WWW under http://dx.doi.org/10.1002/anie.201505294.

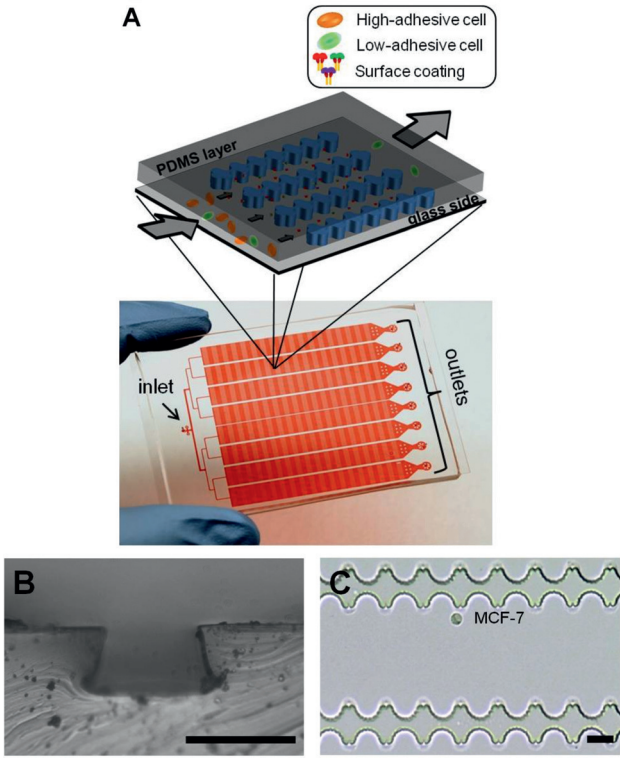

Figure 1. A) Schematic illustration (top) and photograph (bottom) of the high-throughput cell-adhesion chip (HCA-Chip). The chip was filled with a red dye. B) Optical microscopic images of the HCA-Chip. The depth of the microchannel is approximately 25 μm. Scale bar: 30 μm. C) Optical microscopic image of the microchannel structure and a captured MCF-7 cell. Scale bar: 20 μm.

matrix adhesion and natural cellular microenvironments in vivo, we first covered the internal surface of the HCA-Chip with the polystyrene layer and then precoated it with selected biomaterials, such as collagen type I, collagen type IV, and basement membrane extract (BME).[8]

Suspended cells were then applied to the HCA-Chip through a Tygon tube that was connected to the chip inlet. The flow of cells was controlled by a precision syringe pump for a total flow rate of 0.1–2 mL h^{-1}. High-adhesive cells were trapped in the device, and low-adhesive cells were collected from the outlets. After collection of the low-adhesive cells from the outlets, cell dissociation buffer can be used to wash the HCA-Chip, and the high-adhesive cells in the device can be recovered (see Video S1 in the Supporting Information). Cells applied to the HCA-Chip were imaged by fluorescence microscopy. The separated subpopulations were then subjected to cell counting, immunostaining, flow cytometry, a cell invasion assay, or the mammosphere-formation assay. Similar sizes of captured cells were observed in different areas of the chip (see Figure S4). Less than 0.1% of the large-sized cells were trapped at the beginning of the chip.

To demonstrate the separation capacity of the HCA-Chip, we tested two different cancer-cell types: a non-metastatic breast-cancer cell line, MCF-7 (more adhesive), and a metastatic prostate-cancer cell line, VAcP (less adhesive). The cells were spiked into the buffer at varying concentrations, after which they flowed through the HCA-Chip. The high-adhesive cells were captured in the chip, and the low-adhesive cells were collected from the outlets. The capture yield was calculated by counting the number of cells that were loaded into the HCA-Chip and the number of cells that were collected from the outlets. MCF-7 cells (1×10^4–5×10^6 cells mL^{-1}) were then spiked into the buffer solution and captured at a flow rate of 1 mL h^{-1}. There was little difference in capture yield when we increased the number of cells loaded (see Figure S5). Different depths of the microchannel were also applied to find the optimal dimension, and four depths were tested at a flow rate of 1 mL h^{-1}. Because increasing the depth of the microchannel reduced the chance of cells contacting with the functionalized surface and sacrificed the capture yield, an optimized channel depth of 25 μm was used in subsequent experiments (see Figure S6).

Different flow rates were also tested (Figure 2A), and the optimal flow rate was determined to range from 0.2 to 0.5 mL h^{-1}, thus producing a capture yield of over 81.8%. Chips coated with or without different biomaterials were then compared to examine how BME might affect the capture yield. The BME-coated chip exhibited the highest capture yield (Figure 2B; see also Figure S7). To demonstrate the advantage of the HCA-Chip, the BME-coated chip and a commonly used adhesion assay were compared. For both cell lines (MCF-7 and VAcP), the capture efficiency of the HCA-Chip was much higher than that of the adhesion assay. Although almost no VAcP cells were captured in the dish when the adhesion assay was used, about 21.2% of the VAcP cells were trapped in the HCA-Chip (see Figure S6). In comparison to VAcP cells, MCF-7 cells had a higher capture yield in both the HCA-Chip and a commonly used adhesion assay. Our results confirmed the effectiveness of the HCA-Chip in isolating cells on the basis of cell adhesion properties.

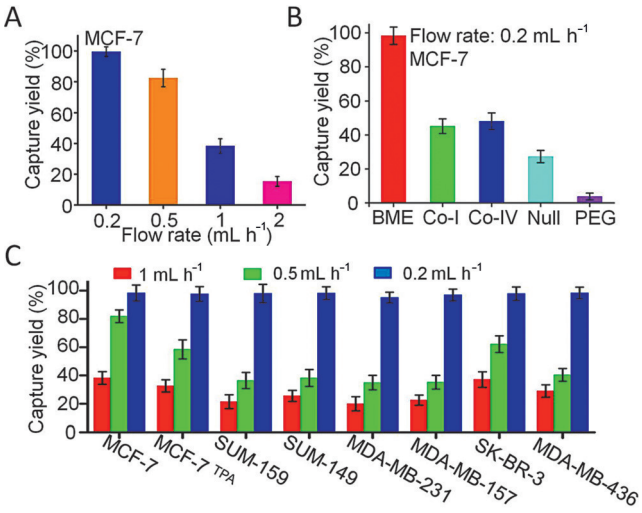

Figure 2. Characterization of the HCA-Chip cell-capture yield for cancer cells in a buffer solution. A) Dependence of MCF-7-capture efficiency on the flow rate. B) Capture of MCF-7 cells in HCA-Chips coated with different biomaterials. C) Comparison of the capture yield of different cell lines in the BME-coated HCA-Chip at different flow rates. Error bars show the standard deviation of three replicates.

To further investigate the relationship between biomaterial coating, capture efficiency, and metastatic capacity, we tested eight different breast-cancer cell lines in the HCA-Chip. MCF-7 and SK-BR-3 cells are less aggressive than SUM-159, SUM-149, MDA-MB-231, MDA-MB-157, and MDA-MB-436 cells.[9] MCF-7 cells were treated with 12-*O*-tetradecanoylphorbol-13-acetate (TPA), a potent tumor promoter, to trigger cell scattering resembling that observed upon epithelial–mesenchymal transition (EMT) and increase the metastatic capacity of the cells (see Figure S8).[10] In the BME-coated chip, MCF-7 and SK-BR-3 cells had higher capture yields when the flow rate was set to 0.5 mL h^{-1}, and small numbers of cells were collected from the outlets. About 81.8% of MCF-7 cells were trapped in the chip. However, the capture yield of MCF-7 was reduced after TPA treatment; only 57.1% of cells were trapped in the chip (Figure 2C). On the contrary, all metastatic breast-cancer cell lines exhibited lower capture yields at 0.5 mL h^{-1}. Even when the flow rate was reduced to 0.2 mL h^{-1}, we collected more metastatic cells from the outlets (see Figure S9). These data indicated that metastatic cells are less adhesive.

These eight breast-cancer cell lines were then tested in chips coated with collagen type I and IV (see Figure S10). Surprisingly, there were no significant differences among these cell lines when the flow rate was set to 0.5 mL h^{-1}. The capture yield of SUM-159 cells in the collagen-coated chip was higher than that in the BME-coated chip (see Figure S11). In polyethylene glycol-coated or uncoated chips, the capture yield was very low. Thus, we coated the surface of the chip with BME in subsequent experiments. The fluid-flow force is the only force to compete with the adhesion between the cell membrane and the coated biomaterial. The adhesion strength is then correlated to the flow rate. In order to isolate the least adhesive cells, the flow rate was set to 0.2 mL h^{-1} in the subsequent separation experiments.

Next, we explored the mechanical subtype of SUM-149 cells in detail. The SUM-149 cell line is known for its intrinsic heterogeneity and is a well-established in vitro model of inflammatory breast cancer.[11] After low-adhesive SUM-149 cells were separated on the basis of cell–substrate adhesion, we assessed the mammosphere-formation efficiency under serum-free conditions in suspension culture to examine

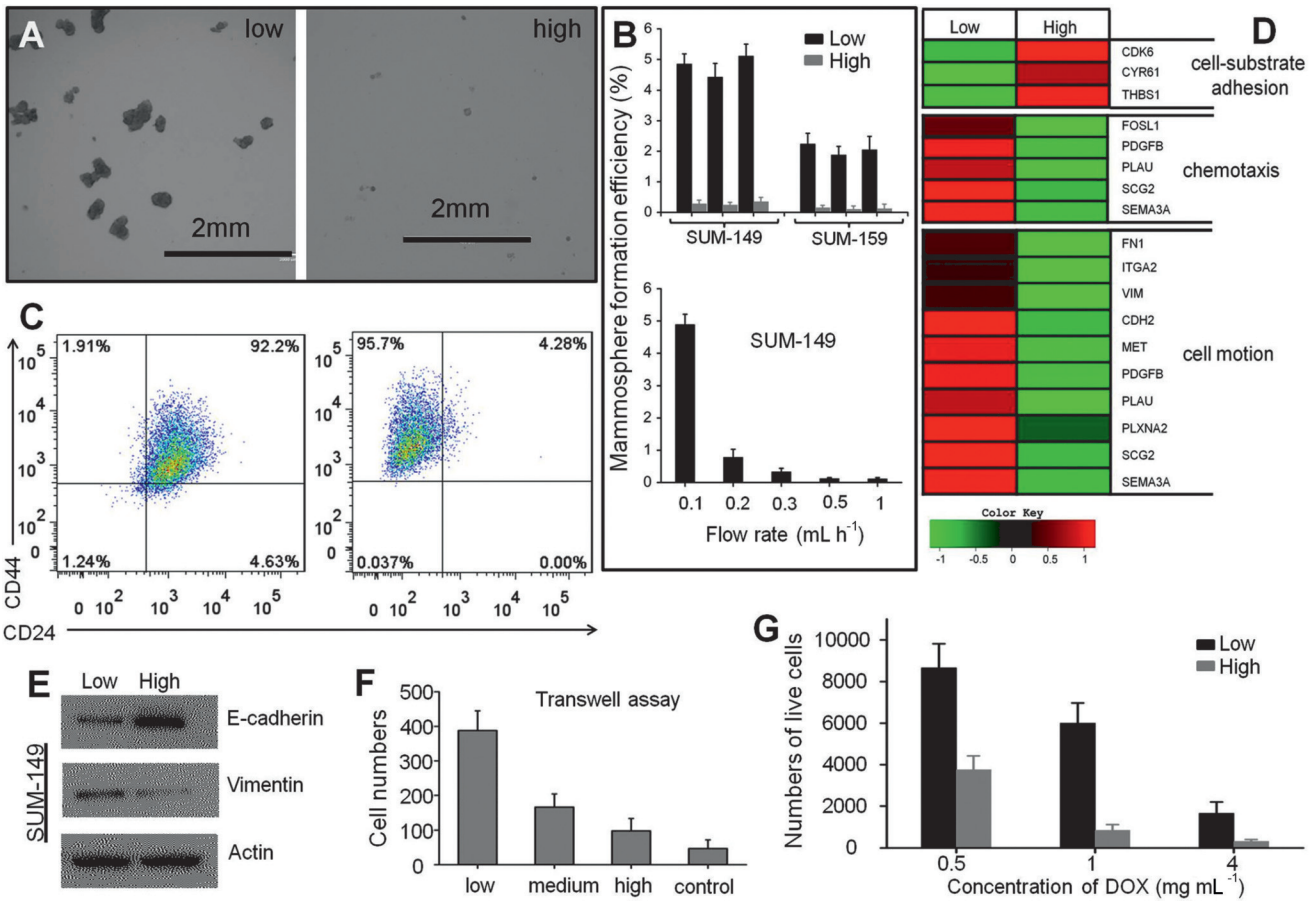

Figure 3. Analysis of the subpopulations of separated cells. A) Mammospheres derived from SUM-149 cells of low and high adhesion. B) Mammosphere-formation efficiency of subpopulations of low and high adhesion. All three replicates showed consistently greater efficiency in flexible cells. C) Scatter plot of CD44/CD24 expression in SUM-149 cells before and after HCA-Chip separation. D) Heat map showing the expression levels of genes related to cell–substrate adhesion, chemotaxis, and cell motion in cells of low and high adhesion. E) Western blot analysis showing E-cadherin and vinmentin production. F) Low-adhesive cells have a higher invasive capacity. G) Resistance of lower and higher adhesive cells to different concentrations of doxorubicin (DOX). The subpopulations of cells were separated 3 times by different HCA-Chips.

tumorigenicity. Less than 1% of tumor cells are able to survive under these culture conditions, and the surviving cells are capable of self-renewal, differentiation, and tumor formation upon transplantation. Results from the mammosphere-formation assay demonstrated that low-adhesive cells exhibited higher growth efficiency and generated larger mammospheres, thus providing functional evidence of TIC enrichment (Figure 3A,B).[11]

To further explore the relationship between low adhesiveness and tumor-initiating features (or CSC likeness), we analyzed the expression of several breast-cancer-stem-cell markers, including CD44, CD24, and epithelial cell adhesion molecule (EpCAM).[12] Flow cytometric analysis confirmed a significant enrichment of the $CD44^+/CD24^-$ (or $CD44^{high}/CD24^-$) population in low-adhesive cells. An increase in the flow rate resulted in a reduced percentage of the $CD44^+/CD24^-$ population (Figure 3C; see also Figure S12). We also tested SUM-159 cells. The data confirmed a significant enrichment of the $CD44^+/EpCAM^+$ (or $CD44^{high}/CD24^-$) population in low-adhesive cells (see Figure S13). Immunofluorescence staining also demonstrated similar results (see Figure S14).

We also applied total RNA-Seq (whole transcriptome) sequencing technology to examine the expression of cancer-metastasis-protein genes in cells with different adhesive properties. Total RNA-Seq can capture a broader range of gene-expression changes and enables the detection of novel transcripts in both coding and noncoding RNAs.[13] The expression profile of the enriched low-adhesive SUM-149 cell subpopulation showed decreased expression levels of genes encoding cyclin-dependent kinase 6, cysteine-rich angiogenic inducer 61, and thrombospondin 1, which are related to cell–substrate adhesion (Cancer Gene Expression Database (CGED)). This finding provides support for the rationale of HCA-Chip separation (Figure 3D).

Our results also indicated that five highly expressed genes are relevant to chemotaxis, and ten highly expressed genes were related to the regulation of tumor-cell migration (Figure 3D). We have previously shown that breast-cancer cells always undergo EMT and acquire increased migratory capabilities.[14] By western blot analysis, we demonstrated that after separation, the low-adhesive cells lost the epithelial marker E-cadherin and gained the mesenchymal marker vimentin (Figure 3E). Because only low-adhesive cells with a substantial fraction of $CD44^+/CD24^-$ cells consistently expressed cell-motion- and chemotaxis-related genes, we compared the invasive capacity of cell lines at different adhesive capacities. Interestingly, low-adhesive cells were more invasive than high-adhesive cells, thus further confirming the association between cell adhesive capacity and invasion (Figure 3F). We also found that low-adhesive cells had a higher survival rate after 24 h of anticancer-drug treatment at the indicated concentrations (Figure 3G).

Next, we used the mammosphere-formation assay to explore whether low-adhesive capacity is related to high metastatic potential in other types of tumor cells. Low-adhesive murine melanoma B16 cells showed higher growth efficiency and generated larger mammospheres, thus providing functional evidence of TIC enrichment (see Figure S15). An in vivo metastatic-lung-tumor model was also generated and assessed. Murine melanoma B16 cells were separated into three subpopulations by the HCA-Chip according to their different adhesive capacities, and then intravenously injected into C57BL/6 mice (1×10^5 cells/mouse). At 18 days after injection, the mice were sacrificed and analyzed for lung

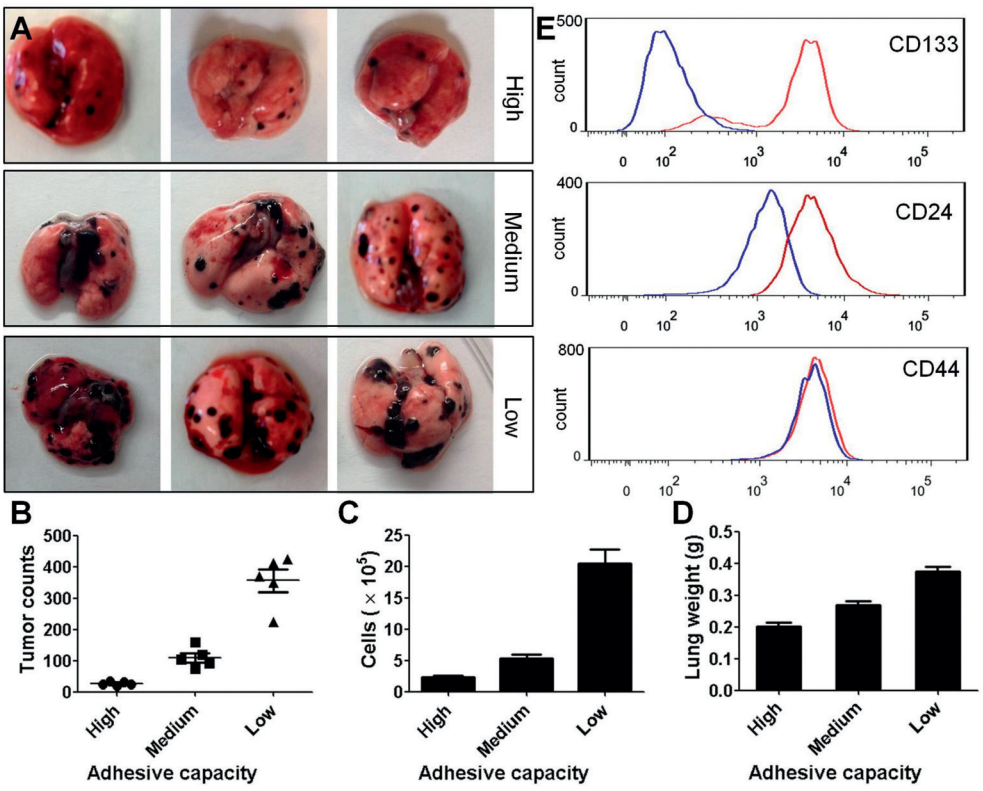

Figure 4. Low-adhesive B16 melanoma cells demonstrated increased potential to induce tumor development. A) Representative images of lungs challenged with high-, medium-, or low-adhesive B16 cells are shown. B–D) The number of tumor foci and the total number of cells in the lung, as well as lung weight, were examined in B6 mice that were challenged with high-, medium-, or low-adhesive B16 cells. D) The expression of CD133, CD24, and CD44 was analyzed in B16 cell subpopulations with different adhesive capacities by flow cytometry (red: after sorting; blue: unsorted).

metastasis. C57BL/6 mice challenged with low-adhesive B16 melanoma cells showed increased tumor development, multiple tumor fusions, higher numbers of tumor foci, and increased lung weight when compared to mice that were challenged with medium- or high-adhesive B16 cells (Figure 4A–C). These data indicate that B16 melanoma cells with lower adhesive capacity have higher metastatic potential, which is consistent with our previous observation in the breast-cancer model. Moreover, hematoxylin and eosin staining showed increased tumor growth in the lungs of C57BL/6 mice challenged with low-adhesive B16 cells, as compared with the medium- or high-adhesive group (see Figures S16–S18). We used flow cytometry to compare the expression of CD133, CD24, and CD44, which are specific cell-surface markers in CSCs, between original B16 melanoma cells and low-adhesive B16 cells. The expression of CD133 and CD24 was increased in the HCA-Chip-isolated, low-adhesive B16 subpopulation as compared to original B16 cells, whereas the expression of CD44 was comparable between groups (Figure 4E).

In summary, we used cell adhesiveness as a biophysical marker to make a tool for CSC isolation. This unique microfluidic sorting method may contribute to the advancement of CSC research and the development of CSC-targeted therapy in a variety of cancer-cell types. The HCA-Chip could potentially be used to purify stem cells and CSCs on the basis of their mechanical characteristics and thereby identify molecular signatures and genes that are essential for tumor initiation. Our device can also be used for tissue samples from cancer patients. Tissue samples often contain many stromal cells and immune cells and limit the CSC-enrichment efficiency. Pre-enrichment, such as separation with magnetic beads, can be used to resolve this problem. We expect that HCA-Chip separation will be useful in a broad range of cancers, even for cancer types for which CSC biomarkers have not yet been discovered.[15]

Keywords: biomaterials · cancer stem cells · cell adhesion · high-throughput methods · microfluidics

How to cite: *Angew. Chem. Int. Ed.* **2015**, *54*, 10838–10842
Angew. Chem. **2015**, *127*, 10988–10992

[1] a) B. Beck, C. Blanpain, *Nat. Rev. Cancer* **2013**, *13*, 727–738; b) L. V. Nguyen, R. Vanner, P. Dirks, C. J. Eaves, *Nat. Rev. Cancer* **2012**, *12*, 133–143.

[2] a) B. B. Zhou, H. Zhang, M. Damelin, K. G. Geles, J. C. Grindley, P. B. Dirks, *Nat. Rev. Drug Discovery* **2009**, *8*, 806–823; b) J. A. McCubrey, L. S. Steelman, S. L. Abrams, N. Misaghian, W. H. Chappell, J. Basecke, F. Nicoletti, M. Libra, G. Ligresti, F. Stivala, D. Maksimovic-Ivanic, S. Mijatovic, G. Montalto, M. Cervello, P. Laidler, A. Bonati, C. Evangelisti, L. Cocco, A. M. Martelli, *Curr. Pharm. Des.* **2012**, *18*, 1784–1795; c) K. Ishizawa, Z. A. Rasheed, R. Karisch, Q. Wang, J. Kowalski, E. Susky, K. Pereira, C. Karamboulas, N. Moghal, N. V. Rajeshkumar, M. Hidalgo, M. Tsao, L. Ailles, T. K. Waddell, A. Maitra, B. G. Neel, W. Matsui, *Cell Stem Cell* **2010**, *7*, 279–282.

[3] V. Tirino, V. Desiderio, F. Paino, G. Papaccio, M. De Rosa, *Methods Mol. Biol.* **2012**, *879*, 513–529.

[4] P. B. Gupta, C. M. Fillmore, G. Jiang, S. D. Shapira, K. Tao, C. Kuperwasser, E. S. Lander, *Cell* **2011**, *146*, 633–644.

[5] a) E. Farahani, H. K. Patra, J. R. Jangamreddy, I. Rashedi, M. Kawalec, R. K. Rao Pariti, P. Batakis, E. Wiechec, *Carcinogenesis* **2014**, *35*, 747–759; b) B. R. Zetter, *Semin. Cancer Biol.* **1993**, *4*, 219–229.

[6] a) Y. Zhang, W. Zhang, L. Qin, *Angew. Chem. Int. Ed.* **2014**, *53*, 2344–2348; *Angew. Chem.* **2014**, *126*, 2376–2380; b) E. Reátegui, N. Aceto, E. J. Lim, J. P. Sullivan, A. E. Jensen, M. Zeinali, J. M. Martel, A. J. Aranyosi, W. Li, S. Castleberry, A. Bardia, L. V. Sequist, D. A. Haber, S. Maheswaran, P. T. Hammond, M. Toner, S. L. Stott, *Adv. Mater.* **2015**, *27*, 1593–1599; c) R. M. Mohamadi, J. D. Besant, A. Mepham, B. Green, L. Mahmoudian, T. Gibbs, I. Ivanov, A. Malvea, J. Stojcic, A. L. Allan, L. E. Lowes, E. H. Sargent, R. K. Nam, S. O. Kelley, *Angew. Chem. Int. Ed.* **2015**, *54*, 139–143; *Angew. Chem.* **2015**, *127*, 141–145.

[7] Y. Zhang, L. Zhou, L. Qin, *J. Am. Chem. Soc.* **2014**, *136*, 15257–15262.

[8] G. Benton, H. K. Kleinman, J. George, I. Arnaoutova, *Int. J. Cancer* **2011**, *128*, 1751–1757.

[9] R. M. Neve, K. Chin, J. Fridlyand, J. Yeh, F. L. Baehner, T. Fevr, L. Clark, N. Bayani, J.-P. Coppe, F. Tong, T. Speed, P. T. Spellman, S. DeVries, A. Lapuk, N. J. Wang, W.-L. Kuo, J. L. Stilwell, D. Pinkel, D. G. Albertson, F. M. Waldman, F. McCormick, R. B. Dickson, M. D. Johnson, M. Lippman, S. Ethier, A. Gazdar, J. W. Gray, *Cancer Cell* **2006**, *10*, 515–527.

[10] W. S. Wu, R. K. Tsai, C. H. Chang, S. Wang, J. R. Wu, Y. X. Chang, *Mol. Cancer Res.* **2006**, *4*, 747–758.

[11] W. J. Zhang, K. Kai, D. S. Choi, T. Iwamoto, Y. H. Nguyen, H. L. Wong, M. D. Landis, N. T. Ueno, J. Chang, L. D. Qin, *Proc. Natl. Acad. Sci. USA* **2012**, *109*, 18707–18712.

[12] C. M. Fillmore, C. Kuperwasser, *Breast Cancer Res.* **2008**, *10*, R25.

[13] C. Trapnell, D. G. Hendrickson, M. Sauvageau, L. Goff, J. L. Rinn, L. Pachter, *Nat. Biotechnol.* **2013**, *31*, 46–53.

[14] R. Kalluri, R. A. Weinberg, *J. Clin. Invest.* **2009**, *119*, 1420–1428.

[15] T. Klonisch, E. Wiechec, S. Hombach-Klonisch, S. R. Ande, S. Wesselborg, K. Schulze-Osthoff, M. Los, *Trends Mol. Med.* **2008**, *14*, 450–460.

Received: June 9, 2015
Published online: July 14, 2015